Theoretical study of the gas phase reaction of methyl acetate with the hydroxyl radical: Structures, mechanisms, rates and temperature dependencies

ARTICLE *in* CHEMICAL PHYSICS LETTERS · APRIL 2010

Impact Factor: 1.9 · DOI: 10.1016/j.cplett.2010.03.031

5 AUTHORS, INCLUDING:

Solvejg Jørgensen
University of Copenhagen
42 PUBLICATIONS **587** CITATIONS
SEE PROFILE

Elna Nilsson
Lund University
47 PUBLICATIONS **340** CITATIONS
SEE PROFILE

Ole John Nielsen
University of Copenhagen
263 PUBLICATIONS **4,912** CITATIONS
SEE PROFILE

Matthew S Johnson
University of Copenhagen
138 PUBLICATIONS **1,683** CITATIONS
SEE PROFILE

Chemical Physics Letters 490 (2010) 116–122

Contents lists available at ScienceDirect

Chemical Physics Letters

journal homepage: www.elsevier.com/locate/cplett

Theoretical study of the gas phase reaction of methyl acetate with the hydroxyl radical: Structures, mechanisms, rates and temperature dependencies

Solvejg Jørgensen *, Vibeke F. Andersen, Elna J.K. Nilsson, Ole John Nielsen, Matthew S. Johnson

Copenhagen Center for Atmospheric Research, Department of Chemistry, University of Copenhagen, Universitetsparken 5, DK-2100 Copenhagen Ø, Denmark

ARTICLE INFO

Article history:
Received 20 January 2010
In final form 15 March 2010
Available online 16 March 2010

ABSTRACT

The reaction mechanism of hydrogen abstraction from methyl acetate by the hydroxyl radical is investigated theoretically. Four hydrogen abstraction reaction channels were found; the OH radical can abstract either the in-plane or the out-of-plane hydrogen atom on either the methyl group or the methoxy group of methyl acetate. There is a ~95% probability that the OH radical abstracts an out-of-plane hydrogen atom from the methoxy group.

1. Introduction

The demand for biofuel is driven by concerns about energy security and climate change. The estimated annual production of commercial biomass by biosynthesis is 170 Gtons [1]. Only 3–4% of this produced biomass is used to produce energy [1]. In an idealized case, biomass used for energy is carbon dioxide (CO_2) neutral; the CO_2 that is removed from air through photosynthesis is released again during energy production. In reality, additional CO_2 is released to the atmosphere since fossil energy is used for farming, transportation and manufacturing [2]. Other greenhouse gas emissions like nitrous oxide (N_2O) can increase due to the use of fertilizers [3].

The production of biofuel has grown rapidly. In Europe, the production of biodiesel increased by 54% in 2006 and 64% in 2005 [4]. Europe produces 73% of biodiesel globally, derived from mainly rapeseed and sunflower [5,6]. Biodiesel is comprised of mono-alkyl esters of long chain fatty acids derived from renewable feed stock like vegetable oils and animal fats. Esters are usually produced by transesterification in which oil/fat reacts with a monohydric alcohol in the presence of a catalyst. Biodiesel has an energy density similar to that of regular diesel, and it is fully miscible with petroleum diesel.

In order to understand the environmental impact of the use of biodiesel, life cycle analysis of a potential biodiesel fuel must be carried out. The final step in the life cycle is combustion. It is expected that 0.01–0.1% of transportation fuel, such as biodiesel is directly emitted to the atmosphere during use [7]. In addition, incomplete combustion produces a variety of chemical compounds in the exhaust including shorter chained methyl esters, aldehydes, and methyl acrylates [8,9].

An additional motivation for the study is to help predict the health impacts of the widespread use of biofuel [10]. Biofuels have a larger oxygen content than liquid hydrocarbons from fossil sources, and it is difficult to predict the reactivity of these compounds. In the atmosphere non-saturated alcohols, ethers and esters are mainly oxidized by the hydroxyl radical, OH. Structure–reactivity relationships are commonly used to predict atmospheric lifetimes, however this method fails for oxygenates [11,12]. For example, the reaction rates with OH predicted using structure reactivity relationships are 3 times too high for 1,3-dioxane, and 2.5 times too high for 2-methoxyethyl ether [11]. Furthermore, the OH radical abstracts a hydrogen atom from oxygenated compounds and often there are several sites for H-abstraction. Each H-abstraction site leads to different reaction products. It is important to know the branching ratio between the different H-abstraction channels in order to predict which biofuel compounds have the most advantageous environmental impact. There is a great interest in discovering the underlying factors causing these unexpected reactivities, which is likely to involve reactant and product complexes.

Here, we focus on the atmospheric fate of methyl acetate $CH_3C(O)OCH_3$ serves as a model system for biodiesel methyl ester reactions. Methyl acetate is oxidized in the atmosphere, mainly by the hydroxyl radical, OH. The reaction rate between methyl acetate and hydroxyl determines the atmospheric lifetime of methyl acetate. The rate coefficients have been determined experimentally [13–17] and theoretically [18]. The results are summarized in Table 1. El Boudali et al. [14] and Wallington et al. [16] performed experiments to determine the temperature-dependent rate coefficient. Both studies showed that the coefficient has a positive temperature dependence. The OH radical can abstract hydrogen from

* Corresponding author.
E-mail address: solvejg@kemi.ku.dk (S. Jørgensen).

0009-2614/$ - see front matter © 2010 Elsevier B.V. All rights reserved.
doi:10.1016/j.cplett.2010.03.031

Table 1
The rate constant (cm^3 $molecule^{-1}$ s^{-1}) for the reaction between methyl acetate and hydroxyl radical obtained experimentally [13–17] and theoretically [18].

Ref.	Methods	Rate constant	Temperature (K)
Experimental observations			
Andersen et al. [13]	Relative rate	$(3.18 \pm 0.13) \times 10^{-13}$	293
El Boudali et al. [14]	Laser photolysis – laser induced fluorescence	$(3.42 \pm 0.09) \times 10^{-13}$	298
Smith et al. [15]	Relative rate	$(3.85 \pm 0.15) \times 10^{-13}$	296
Wallington et al. [16]	Flash photolysis – resonance fluorescence	$(3.41 \pm 0.29) \times 10^{-13}$	296
Campell and Parkinson [17]	Relative rate	$(1.7 \pm 0.5) \times 10^{-13}$	292
Theoretical calculations			
El Boudali et al. [14]	Structure–activity relationship	3.2×10^{-13}	298
Yang et al. [18]	MC-QCISD//MP2/6-311G(d,p)	3.26×10^{-13}	298
This work[a]	CBS-QB3	3.37×10^{-13}	298
This work[a]	CCSD(T)/VTZ//BH&HLYP/aVTZ	4.30×10^{-13}	298
This work[a]	G3	1.10×10^{-12}	298

[a] The reported rate constant include the zero-dimensional Wigner tunneling correction.

either the methoxy ($-OCH_3$) or the methyl ($-CH_3$) group of methyl acetate. Wallington et al. [16] concluded that there is a 95% probability that the OH radical abstracts a hydrogen atom from the $-OCH_3$ group. Furthermore, there are out-of-plane and the in-plane hydrogen atoms on both the $-OCH_3$ and the $-CH_3$ group. In theoretical studies of the reaction mechanism, Yang et al. [18] concluded that out-of-plane H-abstraction from the $-OCH_3$ group is the dominant channel. Yang et al. only considered in-plane H-abstraction for the $-CH_3$ group, however H-abstraction from the $-CH_3$ group only plays a minor role. In this Letter we will study all the four H-abstraction channels. We are especially interested in determining how the branching ratio depends on the level of theory. Our insight in determining the branching ratios for methyl acetate will help to determine the environmental impact of the ongoing increase in the use of oxygenated transportation fuels. In addition, we use methyl acetate as a bench mark for future theoretical investigation for oxygenated compounds.

In this Letter the mechanisms of the H-abstraction reactions between methyl acetate and the OH radical are investigated. The energy profiles for the reaction path for the four H-abstraction channels are calculated using electronic structure theory. We estimate the temperature-dependent rate coefficient for the four reaction channels and the branching ratio.

2. Computational methodology

All calculations were performed using the Gaussian 03 programs [19]. Optimized geometries and the corresponding energies for the reactants, reactant complexes, transition state structures, product complexes and products are determined with density functional theory BH&HLYP [20,21] with the basis sets, 6-31+G(d) [22,23] and aug-cc-pVTZ [24], which is denoted as aVTZ. It has previously been shown that BH&HLYP is suitable to predict the geometries and frequencies of the transition state structure [25]. The calculated frequencies are used to characterize the nature of a stationary point (a minimum or a saddle point) and to estimate the zero-point vibrational energy (ZPE). Furthermore, at the BH&HLYP/6-31+G(d) level of theory we have verified by intrinsic reaction coordinate (IRC) calculations [26,27] that the transition state connects the chosen reactant and product complexes.

To obtain reliable energies at each stationary point, a single point energy optimization was performed using the BH&HLYP/aVTZ geometries. We used two *ab initio* methods with the cc-pVTZ basis set [24]; (i) the second order perturbation theory of Møller-Plesset (PMP2) [28] and (ii) the coupled cluster single and double method including a perturbative estimate of triples (CCSD(T)) [29]. For open-shell species spin projected MP2 (PMP2) energies were used, since it has been shown that PMP2 values yield energy differences that are in far better agreement with experimental values than similar calculations without PMP2 [30]. In order to obtain the total energies, both the MP2 and CCSD(T) energies are corrected with zero-point energies from the BH&HLYP/aVTZ level of theory. Furthermore, Gaussian 3 level of theory (G3) [31] and CBS-QB3 [32,33] have been used to optimize and refine the energy.

The major problem in the application of the unrestricted calculations is spin contamination from higher lying spin states. At the UBH&HLYP level of theory for both basis sets, the expectation value of the total spin is less than 0.77 before spin annihilation, and 0.75 after spin annihilation. Concerning the UMP2 calculation, the expectation value of the total spin is less than 0.80 before spin annihilation and it is almost 0.75 after spin annihilation. Similar trend is observed for the G3 and CBS-QB3 calculations. Therefore, spin contamination is not considered to be severe. In general, spin contamination for the transition state structures and the product complexes was larger than for the reactant complexes.

3. Results and discussion

3.1. Reaction mechanism

The OH radical can abstract a hydrogen atom from either the methoxy group i.e. the $-OCH_3$ group

$$CH_3C(O)OCH_3 + OH \rightarrow CH_3C(O)OCH_2 + H_2O \quad (1)$$

or the methyl group i.e. the $-CH_3$ group.

$$CH_3C(O)OCH_3 + OH \rightarrow CH_2C(O)OCH_3 + H_2O. \quad (2)$$

Hydrogen abstraction can be divided into in-plane and out-of-plane H-abstraction reactions. Reaction paths 1a and 2a are in-plane H-abstractions on the methoxy and methyl groups respectively, whereas reaction paths 1b and 2b are out-of-plane H-abstraction reactivities. Yang et al. [18] considered only the in-plane H-abstraction from $-CH_3$ group (path 2a).

All geometries of the reactant complexes (**RC**), transition state structures (**TS**) and product complexes (**PC**) at the BH&HLYP/aVTZ level of theory are shown in Figs. 1 and 2 for the H-abstraction on the methoxy group (reaction path 1a and 1b) and the methyl group (reaction path 2a and 2b), respectively.

The relative energies of the reactants, $CH_3C(O)OCH_3 + OH$, are shown for the stationary points along the reaction path for the different levels of theory in Table 2. Tables S1 and S2 of the Supplementary material tabulate the electronic and zero-point vibrational energies of the studied method.

3.1.1. Reactant complexes

The reactant complex **RC1b** initializing the out-of-plane H-abstraction is stabilized by a strong H-bond between the hydrogen atom in the OH radical and the oxygen atom in the carbonyl

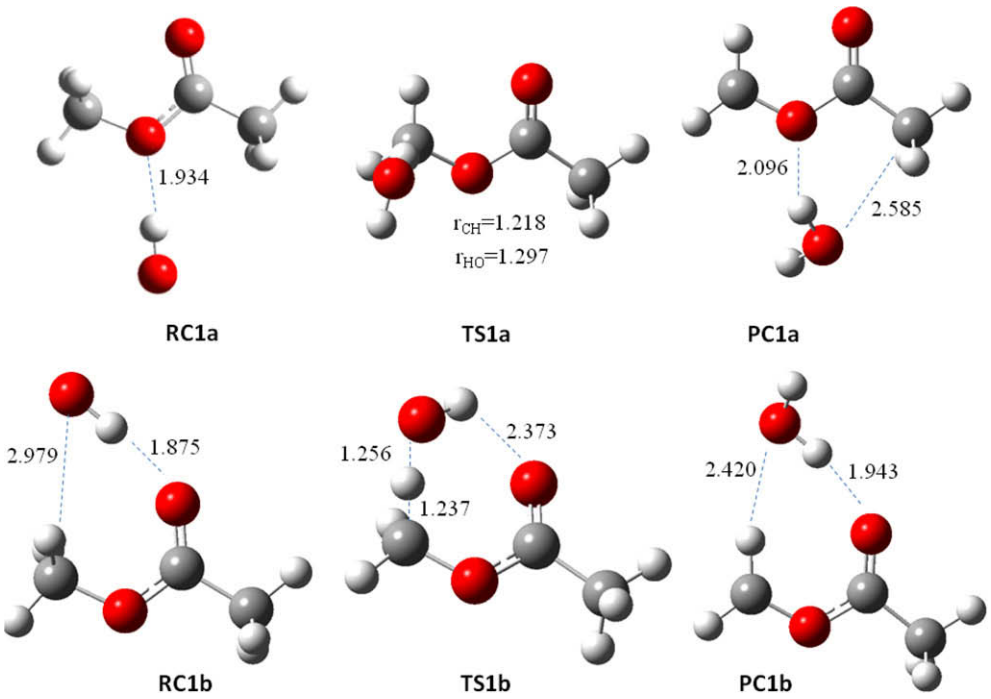

Fig. 1. Optimized geometries for the reactant complexes (**RC**), transition state structures (**TS**) and product complexes (**PC**) for the reaction path, $CH_3C(O)OCH_3 + OH \rightarrow CH_3C(O)OCH_2 + H_2O$ obtained at the BH&LYP/aVTZ level of theory. The reaction paths 1a and 1b correspond to the in-plane and the out-of-plane H-abstraction respectively. The bond lengths are given in Ångstrøms.

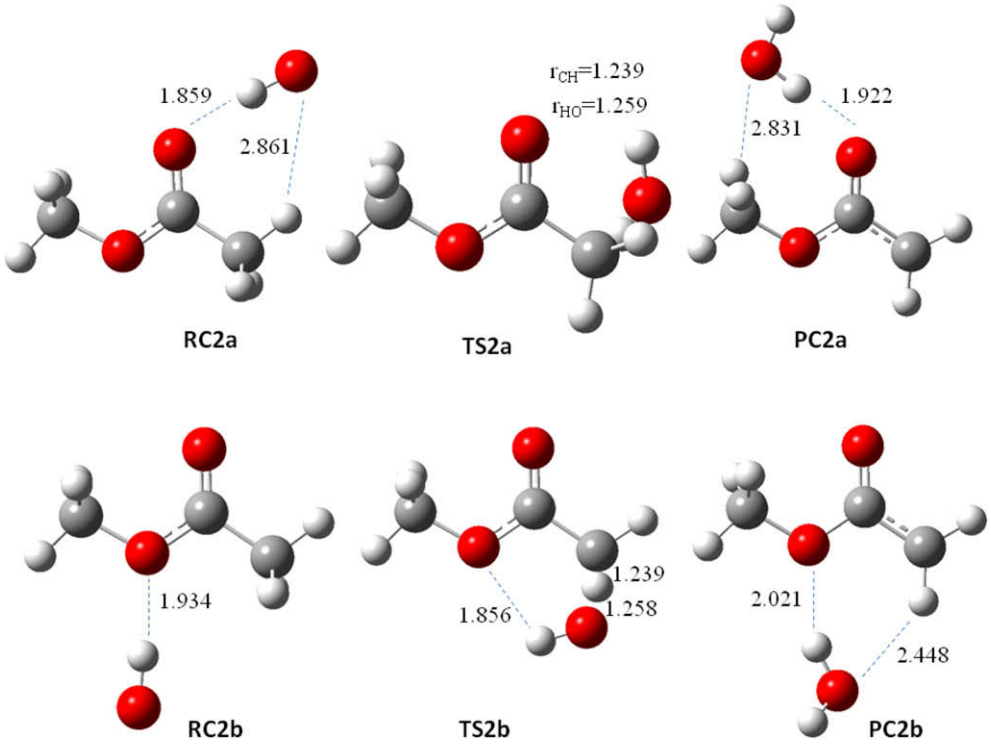

Fig. 2. The optimized geometries for the reactant complexes (**RC**), transition state structures (**TS**) and product complexes (**PC**) for the reaction path, $CH_3C(O)OCH_3 + OH \rightarrow CH_2C(O)OCH_3 + H_2O$ obtained at the BH&LYP/aVTZ level. The reaction paths 2a and 2b correspond to the in-plane and the out-of-plane H-abstraction, respectively. The bond lengths are given in Ångstrøms.

group with the length 1.88 Å at BH&HLYP/aVTZ level of theory. There are two weaker interactions between the oxygen atom in the OH radical and the two out-of-plane hydrogen atoms on the methoxy group. Concerning the reactant complex for the in-plane H-abstraction on the methoxy group **RC1a**, there is only an H-bond between the hydrogen atom in the OH radical and the ether linkage –O– with the length 1.93 Å at BH&HLYP/aVTZ, therefore **RC1a** is less stabilized than **RC1b**. Both G3 and CBS-QB3 predict

Table 2
Energies corrected for zero-point vibrational energy relative to the reactant of the reactant complexes (**RC**), transition state structures (**TS**), product complexes (**PC**) and product (**P**) in the H-abstraction reaction, $CH_3C(O)OCH_3$ + OH, for various level of theory. The energies are given in kJ/mol. In the single point energy calculation at MP2 and CCSD(T) we have used the zero-point vibrational energies obtained at BH&HLYP/aVTZ.

Path	Method	RC	TS	PC	P
1a	BH&HLYP/6-31+G(d)	−14.99	34.92	−50.82	−41.09
	BH&HLYP/aVTZ	−10.59	27.29	−69.09	−63.11
	MP2/VTZ//BH&HLYP/aVTZ	−16.46	11.22	−100.42	−87.16
	CCSD(T)/VTZ//BH&HLYP/aVTZ	–	13.77	–	−71.76
	G3	−14.10	14.23	−86.91	−76.06
	CBS-QB3	−12.37	14.45	−87.74	−81.28
1b	BH&HLYP/6-31+G(d)	−22.14	26.73	−60.37	−41.09
	BH&HLYP/aVTZ	−20.13	30.23	−77.70	−63.11
	MP2/VTZ//BH&HLYP/aVTZ	−23.32	−2.73	−106.61	−87.16
	CCSD(T)/VTZ//BH&HLYP/aVTZ	–	1.97	–	−71.76
	G3	−20.66	2.91	−91.83	−76.06
	CBS-QB3	−18.50	−0.45	−93.41	−81.28
2a	BH&HLYP/6-31+G(d)	−25.00	37.44	−70.76	−49.67
	BH&HLYP/aVTZ	−21.14	30.21	−84.34	−67.24
	MP2/VTZ//BH&HLYP/aVTZ	−23.82	7.37	−112.01	−90.88
	CCSD(T)/VTZ//BH&HLYP/aVTZ	–	13.73	–	−73.60
	G3	−21.93	14.38	−104.48	−82.84
	CBS-QB3	−20.73	9.37	−99.00	−84.76
2b	BH&HLYP/6-31+G(d)	−14.99	37.43	−63.37	−49.67
	BH&HLYP/aVTZ	−10.59	30.84	−76.38	−67.24
	MP2/VTZ//BH&HLYP/aVTZ	−16.46	7.29	−106.74	−90.88
	CCSD(T)/VTZ//BH&HLYP/aVTZ	–	13.57	–	−73.60
	G3	−14.10	14.58	−96.06	−82.84
	CBS-QB3	−12.37	10.61	−95.74	−84.76

longer H-bond in the **RC1a** and **RC1b** whereas the distance for the weaker interactions between the oxygen atom in the OH radical and the two out-of-plane hydrogen atoms on the methoxy group is shorter in the G3 and CBS-QB3 calculation than in the BH&HLYP/aVTZ calculation. The values are 2.98, 2.57 and 2.67 Å for BH&HLYP, G3 and CBS-QB3 level of theory. The energy difference between the two reactant complexes, **RC1a** and **RC1b**, is 6.1 kJ/mol at the CBS-QB3 level of theory.

The opposite trend is observed in the reactant complexes for H-abstraction on the methyl group, denoted as **RC2a** and **RC2b**. The in-plane reactant complex **RC2a** is better stabilized than the out-of-plane reactant complex **RC2b**; the energy difference is 8.3 kJ/mol at the CBS-QB3 level of theory. **RC2a** has an H-bond between the hydrogen atom in the OH radical and the oxygen atom in the carbonyl group with length 1.86 Å at BH&HLYP/aVTZ and a weak interaction between the oxygen atom in the OH radical and the in-plane hydrogen atom on the methyl group with length 2.86 Å at BH&HLYP/aVTZ. G3 and CBS-QB3 predict longer H-bond and shorter distance for the weak interactions. The reactant complexes, **RC1a** and **RC2b,** are almost identical. The same reactant complex can either lead to in-plane H-abstraction on the methoxy group or out-of-plane H-abstraction on the methyl group.

Comparing the reactant complexes, **RC1b** and **RC2a**, they are stabilized by the H-bonded network leading to the formation of a ring-like structure. The reactant complexes **RC1b** and **RC2a** are similar as both of them have a hydrogen bond between the H in the OH radical and the O in carbonyl group. **RC1b** has a hydrogen bond between the oxygen atom in the OH radical and the out-of-plane hydrogen atom of the $-OCH_3$ group whereas **RC2a** has a hydrogen bond to the in-plane hydrogen atom of the $-CH_3$ group. The weak interactions in **RC2a** are shorter than in **RC1b**, therefore **RC2a** is better stabilized than **RC1b** relative to the separated reactants. The energy differences are 1.3 and 2.2 kJ/mol at the G3 and CBS-QB3 level of theory, respectively. We also observe that the hydrogen bond between the hydrogen atom in the OH radical and the oxygen in the carbonyl group is stronger/shorter (**RC1b** and **RC2a**) than the one between the hydrogen atom in the OH radical and the oxygen in the ether linkage (**RC1a** and **RC2b**).

3.1.2. Transition state structures

The transition state structures are denoted **TS1a** and **TS1b** for the in-plane and the out-of-plane H-abstraction on the methoxy group, respectively. At the CBS-QB3 level of theory, the energy barriers are 26.8 and 18.1 kJ/mol for the in-plane and the out-of-plane H-abstraction, the G3 calculation predict higher barriers. The transition state of the out-of-plane H-abstraction **TS1b** has a lower energy barrier primarily due to a hydrogen bond between the hydrogen atom in the OH group and the oxygen in the carbonyl group. The length of the breaking bond between C and H is 1.22 and 1.24 Å in **TS1a** and **TS1b**, respectively, whereas the distances are 1.30 and 1.26 Å for the forming bond between H and O in **TS1a** and **TS1b**, respectively. H-abstraction happens earlier for the in-plane than for the out-of plane H-abstraction reaction path. **TS1a** is more reactant complex-like than **TS1b**.

Concerning H-abstraction on the methyl group, the energy barriers at the CBS-QB3 level of theory are 30.2 and 23.0 kJ/mol for in-plane and the out-of-plane H-abstraction, respectively. Again CBS-QB3 predicts lower barrier height than G3 level of theories. The lengths of the bond breaking and bond forming positions are similar for the two transition state structures, **TS2a** and **TS2b**. The differences in the two transition state structures are in the orientation of the OH radical relative to the carbonyl group/ether linkage. In **TS1a** the distance between the hydrogen atom in the OH group and the oxygen atom in the carbonyl group is 3.07 Å whereas the distance between the hydrogen atom in the OH group and the oxygen in the ether linkage is 1.86 Å.

In general, the energy barriers for BH&HLYP tend to be higher than for MP2. Concerning out-of-plane H-abstraction on the methoxy group MP2 predicts that the energy of the transition state structure is below the energy of the reactants whereas the other methods predict it to be above the energy of the reactants, $CH_3C(O)OCH_3$ and OH.

3.1.3. Product complexes

A product complex is formed between water and the radical, either $CH_3C(O)OCH_2$ or $CH_2C(O)OCH_3$. The energy differences between **PC1a** and **PC1b** are 4.9 and 5.6 kJ/mol at G3 and CBS-QB3 level of theory. **PC1b** is better stabilized than **PC1a** due to the fact that the interaction between H_2O and the radical is stronger e.g. the distance in **PC1b** between hydrogen in water and oxygen in the carbonyl group is 1.94 Å, whereas the distance in **PC1a** between water and the ether linkage is 2.10 Å. A similar trend is observed for **PC2a** and **PC2b**.

3.2. Reaction rate constant

In the previous section it was shown that the reaction pathways for H-abstraction consist of a reversible first step involving the barrierless formation of a reactant complex, followed by the irreversible formation of products. Each reaction pathway is a two-step process with the corresponding reactant complex in equilibrium with the reactants

$$CH_3C(O)OCH_3 + OH \underset{k_{-1,i}}{\overset{k_{1,i}}{\leftrightarrow}} \text{reactant complex } (\mathbf{RCi}) \overset{k_{2,i}}{\rightarrow} \text{product}. \quad (3)$$

We assume that $k_{1,i}$ and $k_{-1,i}$ are the rate constants for the first step and $k_{2,i}$ is the rate constant of the second step of the ith reaction path. A steady-state analysis leads to the rate constant for the overall reaction

$$k_i = \frac{k_{1,i}k_{2,i}}{k_{-1,i} + k_{2,i}}. \quad (4)$$

Table 3
The imaginary frequency v_i (cm^{-1}), the zero-dimensional Wigner tunneling correction Γ_i (dimensionless), the rate constant k_i (cm^3 $molecule^{-1}$ s^{-1}), the branching ratio without tunneling correction k_i/k_{notun} (dimensionless) the branching ratio with tunneling correction $\Gamma_i k_i/k_{tun}$ (dimensionless) for the four H-abstraction are channels are shown for various level of theory, where $k_{notun} = k_{1a} + k_{1b} + k_{2a} + k_{2b}$ and $k_{tun} = \Gamma_{1a}k_{1a} + \Gamma_{1b}k_{1b} + \Gamma_{2a}k_{2a} + \Gamma_{2b}k_{2b}$. The results are given at 298 K.

Path	Method	v_i	Γ_i	k_i	k_i/k_{notun}	Γ_i k_i/k_{tun}
1a	BH&HLYP/6-31+G(d)	1912i	4.54	4.23×10^{-19}	8.5	7.5
	BH&HLYP/aVTZ	1638i	3.75	8.35×10^{-18}	12.3	10.2
	MP2/VTZ//BH&HLYP/aVTZ	1638i	3.75	5.45×10^{-15}	0.9	0.7
	CCSD(T)/VTZ//BH&HLYP/aVTZ	1638i	3.75	1.94×10^{-15}	2.1	1.7
	G3	3213i	11.02	2.95×10^{-15}	3.1	3.0
	CBS-QB3	361i	1.13	2.42×10^{-15}	1.3	0.8
1b	BH&HLYP/6-31+G(d)	2087i	5.23	4.36×10^{-18}	87.2	88.2
	BH&HLYP/aVTZ	1926i	4.60	5.64×10^{-17}	83.0	85.0
	MP2/VTZ//BH&HLYP/aVTZ	1926i	4.60	5.90×10^{-13}	93.2	93.5
	CCSD(T)/VTZ//BH&HLYP/aVTZ	1926i	4.60	8.90×10^{-14}	94.8	95.2
	G3	3268i	11.36	9.15×10^{-14}	94.5	94.6
	CBS-QB3	925i	1.83	1.77×10^{-13}	96.2	96.3
2a	BH&HLYP/6-31+G(d)	2094i	5.26	1.10×10^{-19}	2.2	2.2
	BH&HLYP/aVTZ	1911i	4.54	1.63×10^{-18}	2.4	2.4
	MP2/VTZ//BH&HLYP/aVTZ	1911i	4.54	1.63×10^{-14}	2.6	2.5
	CCSD(T)/VTZ//BH&HLYP/aVTZ	1911i	4.54	1.26×10^{-15}	1.3	1.3
	G3	3269i	11.37	1.07×10^{-15}	1.1	1.1
	CBS-QB3	1239i	2.49	1.73×10^{-15}	1.0	1.3
2b	BH&HLYP/6-31+G(d)	2077i	5.18	1.05×10^{-19}	2.1	2.1
	BH&HLYP/aVTZ	1912i	4.55	1.59×10^{-18}	2.3	2.4
	MP2/VTZ//BH&HLYP/aVTZ	1912i	4.55	2.11×10^{-14}	3.3	3.3
	CCSD(T)/VTZ//BH&HLYP/aVTZ	1912i	4.55	1.68×10^{-15}	1.8	1.8
	G3	3263i	11.33	1.31×10^{-15}	1.3	1.3
	CBS-QB3	981i	1.93	2.79×10^{-15}	1.5	1.6

We assume that the rate constant $k_{-1,i}$ for transforming the reactant complex into the reactants is much faster than the rate constant $k_{2,i}$ transforming the reactant complex into the products. The rate constant for Eq. (3) is then $k_i = K_{eq,i}k_2$ where the equilibrium constant is given by $K_{eq,i} = k_{1,i}/k_{-1,i}$. Thereby we do not need to estimate the forward and reverse rate constants for the first step. Under this assumption the rate constant of the ith reaction path can be estimated by conventional transition state theory [34] given by

$$k_i(T) = K_{eq,i}(T)k_{2,i}(T) = \sigma_i \frac{k_b T}{h} \frac{Q_{TSi}}{Q_M Q_{OH}} \exp\left(-\frac{E_{TSi} - (E_M + E_{OH})}{k_b T}\right), \quad (5)$$

where h is the Planck constant and the energy $E_{TSi} - (E_M + E_{OH})$ is the energy barrier between the individual reactants and the transition state. $CH_3C(O)OCH_3$ is denoted by M in Eq. (4). The constant σ_i is the symmetry factor counting the number of possible identical reaction paths. For the in-plane H-abstraction the symmetry factor σ_i is one (reaction path 1a and 2a) whereas it is two for the out-of-plane H-abstraction (reaction path 1b and 2b). Partition functions Q are evaluated using the standard procedure involving translational, rotational, vibrational and electronic contributions. The OH radical has two low lying electronic states $^2\Pi_{3/2}$ and $^2\Pi_{1/2}$, the energy difference between the two electronic states is approximately 140 cm^{-1} [35]. The electronic partition for the OH radical is $Q_e = 2 + 2\exp(-140/k_bT) = 3.019$. The moments of inertia and vibrational frequencies are summarized in Tables S3–S6 of Supporting Information.

Under the assumption that $k_{2,i} << k_{-1,i}$ the reactant complexes do not enter into the overall rate constant. In most cases the transition state is higher in energy than the individual reactants with the exception of path 1b calculated at the MP2/cc-pVTZ//BH&HLYP/apVTZ and CBS-QB3 level of theory. In all the studied cased the difference in Gibbs energy between the transition state and the individual reactants at 298 K are greater than zero.

The temperature dependent tunneling correction $\Gamma_i(T)$ represents quantum mechanical tunneling and it is implemented for using the one-dimensional Wigner tunneling correction [36]

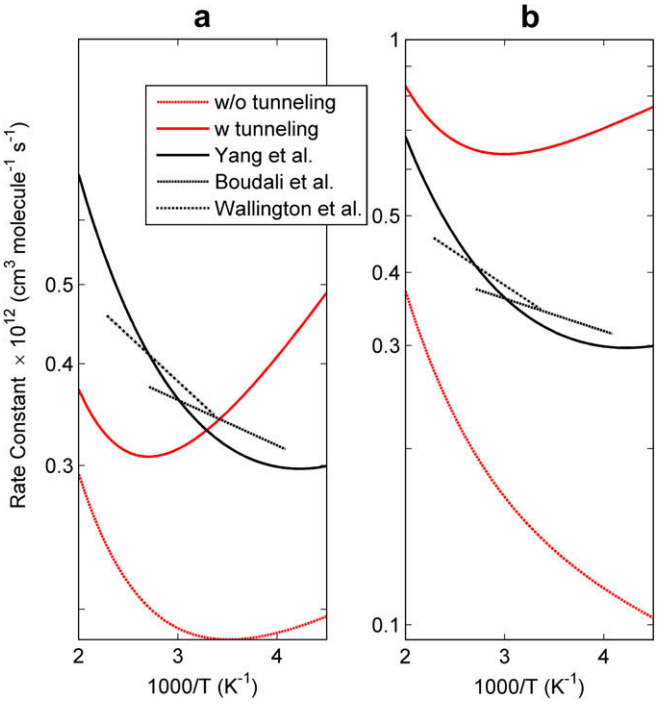

Fig. 3. The total rate constant without tunneling correction (red dashed) and with tunneling correction (red solid) for the H-abstraction reaction, $CH_3C(O)OCH_3$ + OH obtained at the (a) CBS-QB3 and (b) CCSD(T)/cc-pVTZ//BH&HLYP/aVTZ level of theories. Comparison of the total rate constants and the experimental values. (For interpretation of the references to colour in this figure legend, the reader is referred to the web version of this article.)

$$\Gamma_i(T) = 1 + \frac{1}{24}\left(\frac{hv_i}{k_b T}\right)^2, \quad (6)$$

where v_i is the imaginary frequency representing the curvature of the potential energy surface at the transition state for the ith

H-abstraction channel. $\Gamma_i(T)$ is a dimensionless number, with a limiting value of 1 as T approaches infinity. The imaginary frequencies of the transition state structures TS1a, TS1b, TS2a, and TS2b are 1683i, 1926i, 1911i and 1912i cm^{-1}, respectively, obtained using BH&HLYP/aVTZ. At 298 K the one-dimensional Wigner tunneling correction ranges from 3.75 to 4.60 (see Table 3). In the G3 calculation the vibrational frequencies are calculated at the HF/6-31G(d) level of theory. The imaginary frequencies are on the order of 3250 cm^{-1}. The CBS-QB3 level of theory calculates the vibrational frequencies with B3LYP/CBSB7. The imaginary frequencies from CBS-QB3 calculations are smaller than the BH&HLYP/aVTZ.

Table 3 lists rate constants without tunneling correction for the four H-abstraction channels calculated at 298 K for various methods. We observe that a difference of 20 kJ/mol in the energy barrier leads to a deviation of 1000 cm^3 $molecule^{-1}s^{-1}$ in the rate constant. It is therefore important to estimate the energy barrier with good accuracy. The total rate constant for H-abstraction, $CH_3C(O)OCH_3$ + OH, associated with the four H-abstraction channels is $k_{notun} = k_{1a} + k_{1b} + k_{2a} + k_{2b}$ and $k_{tun} = \Gamma_{1a}\ k_{1a} + \Gamma_{1b}\ k_{1b} + \Gamma_{2a}\ k_{2a} + \Gamma_{2b}\ k_{2b}$ without and with the one-dimensional Wigner tunneling correction, respectively. We have computed the branching ratio for the four H-abstraction channels. At all levels of theory, the out-of-plane H-abstraction from the methoxy group (reaction path 1b) has the largest branching ratio. We observed that the branching ratio including the tunneling factors deviates very little from the branching ratio without the tunneling factors, this is because the differences in the tunneling correction for the different H-abstraction channels are very small. The MP2/cc-pVTZ//BH&HLYP/aVTZ, CCSD(T)/cc-pVTZ//BH&HLYP/aVTZ, G3 and CBS-QB3 levels of theory predict the same magnitude of branching ratio. At 298 K, the probability of out-of-plane H-abstraction from the methoxy group is estimated at 96% for CBS-QB3 level of theory. The estimated probability of the in-plane H-abstraction from both the methoxy the methyl group is 1% whereas, it is 2% from the out-of-plane H-abstraction from the methyl group. These estimates are in good agreement with Wallington et al. [16], who concluded from their product analysis that there is a 95% probability of the OH radical abstracting a hydrogen atom from the methoxy group. Yang et al. [18] also concluded that the out-of-plane H-abstraction from the methoxy group is the dominant channel. This reaction path dominates since there is a hydrogen bond between the hydrogen atom in the OH group and the oxygen in the carbonyl group of the transition state structure (**TS1b**) leading to the lowest energy barrier of the four H-abstraction reaction paths.

In Table 1 the overall rate constant with tunneling correction at 298 K is tabulated for various methods. Yang et al. [18] compute the energy of the stationary points along the reaction path at the MC-QCIST//MP2/6-311G(d,p) level of theory. They estimated the overall rate constant using canonical variation transition state theory including the curvature of the potential energy surface at the transition state; this calculation requires information from an intrinsic reaction coordinate (IRC) calculation. The overall rate constant at the CBS-QB3 level of theory predicts the experimentally measured values whereas CCSD(T)/cc-pVTZ//BH&HLYP/aVTZ overestimates the overall rate constant by 33%.

In Fig. 3 the total rate constant with and without tunneling correction is shown as a function of temperature for the CBS-QB3 and CCSD(T)/cc-pVTZ//BH&HLYP/aVTZ levels of theory. Only the total rate constant at the CCSD(T)/cc-pVTZ//BH&HLYP/aVTZ level of theory exhibits a positive temperature dependence, which is also measured experimentally [14,16]. El Boudali et al. measured the total rate constant in the temperature range 243–369 K, and Wallington et al. in the range 240–440 K. Only the CCSD(T)/cc-pVTZ//BH&HLYP/aVTZ correctly describes the feature of the surface, but it is shifted relative to the results obtained by Yang et al. [18]. If we compare our calculated total rate constants at the CCSD(T)/cc-pVTZ//BH&HLYP/aVTZ level of theory with the experimental value, the total rate constant without tunneling correction underestimates the reaction rate whereas the one with tunneling correction overestimates the rate. The error in the no-tunneling rate is more pronounced at low temperatures, where tunneling plays a more important role. We can therefore conclude that tunneling plays an important role in the true rate constant. Even through the rate constant at the CBS-QB3 level, including tunneling, predicts the measured rate constant. This could be because the imaginary frequencies for the CBS-QB3 calculation are lower than for the BH&HLYP/aVTZ level of theories leading to larger deviation in the tunneling corrections. We can conclude that only the expensive CCSD(T) level of theory of the studied methods is able to predict the behavior of the overall rate constant. Transition state theory correctly predicts the magnitude of the overall rate constant, but the one-dimensional Wigner tunneling correction overestimates the quantum correction.

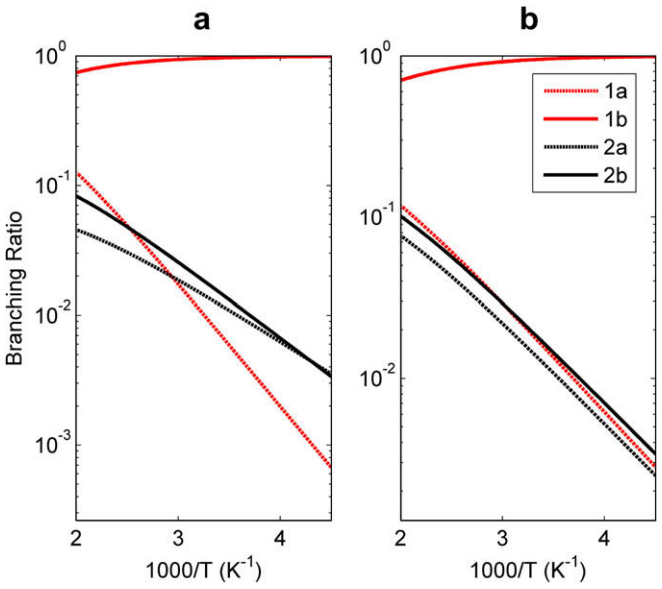

Fig. 4. The temperature dependent branching ratio for the H-abstraction reaction, $CH_3C(O)OCH_3$ + OH. The results are obtained at the (a) CBS-QB3 and (b) CCSD(T)/cc-pVTZ//BH&HLYP/aVTZ level of theories.

Fig. 4 shows the branching ratio including the tunneling correction for the *i*th reaction path as a function of time for the CBS-QB3 and CCSD(T)/cc-pVTZ//BH&HLYP/aVTZ levels of theory. The two methods predict the same overall behavior. The branching ratio indicates that out-of-plane H-abstraction from the methoxy group dominates over the temperature range studied. The probability of H-abstraction in out-of-plane H-abstraction decreases with increasing temperature whereas the opposite is observed for the other reaction channels.

4. Conclusion

We have investigated the reaction mechanism and kinetics of the H-abstraction reaction of $CH_3C(O)OCH_3$ + OH. We have observed four reaction paths; they describe in-plane and out-of-plane H-abstraction on either the methoxy group ($-OCH_3$) or the methyl group ($-CH_3$). We have succeeded in locating the pre- and post-reaction complexes in the reaction mechanism. We have calculated the rate constant using standard transition state theory. We estimated the rate constants for the individual reaction paths and the overall reaction rate constant. The overall rate constant shows a positive temperature dependence which is also observed

experimentally. The calculated overall rate constant is in good agreement with experimental value. From the calculated rate we can estimate the branching ratio between the reaction channels. Considering the branching ratio, we can conclude that the probability that the OH radical abstracts a hydrogen atom out of the plane of the methoxy group is ~96% and therefore the dominant channel. This reaction channel dominates since both the reactant complex and transition state structure are stabilized by three H-bonds, forming a seven member ring-like structure. The OH radical abstracts ~1% from the in-plane H on the methoxy group and methyl group and ~2% from the out-of-plane H on the methyl group. We have considered the four H-abstraction channels. An earlier study by Yang et al. [18] did not consider the out-of-plane H-abstraction from the $-CH_3$ group; we predict there is a probability of 2% of abstraction of the out-plane H from the $-CH_3$ group.

El Boudali et al. [14] used the structure activity relationship (SAR) of Kwok and Atkinson [11] to estimate the rate constant between methyl acetate and the hydroxyl radical. The SAR-estimated rate constant is 3.2×10^{-13} cm^3 molecule^{-1} s^{-1}, which is in good agreement with experimental values. In the current SAR database one cannot distinguish between out-of-plane and in-plane H-abstraction for both the methoxy and methyl group of methyl acetate. Only quantum mechanical calculations of the detailed reaction mechanism provide this insight. We observe that the branching ratio including the tunneling factors deviates very little from the branching ratio without the tunneling factors. The MP2/cc-pVTZ//BH&HLYP/aVTZ, CCSD(T)/cc-pVTZ//BH&HLYP/aVTZ, G3 and CBS-QB3 levels of theory predict the same magnitude of branching ratio. Only CCSD(T)/cc-pVTZ//BH&HLYP/aVTZ predicts the temperature behavior of the overall rate constant.

The reaction between methyl acetate and the OH radical serves as a benchmark for investigations of longer branched and unbranched methyl esters as well as acetates. Cheaper computational methods like G3 and CBS-QB3 may be used to predict the branching ratio but CCSD(T) is recommended for computing the overall rate constant. We observed that the calculated branching ratio is in good agreement with the experimental observation. This insight will help in future work to determine the environmental impact of the ongoing increase in the use of oxygenated transportation fuels, i.e. biofuels.

We assume that the rate constant $k_{-1,i}$ for transforming the reactant complex into the reactants is much faster than the rate constant k_2 transforming the reactant complex into products. In this way we avoid estimating the forward and reverse rate constants for the first step which involves a fast pre-equilibrium between the reactants and the pre-reactive complex. Since the formation of the reactant complex proceeds without a barrier, the location of the transition state could be determined variationally by minimizing the reaction rate [37].

Acknowledgements

Danish Center for Scientific Computing (DCSC) and the Copenhagen Center for Atmospheric Research (CCAR) are acknowledged for their support. CCAR is supported by the Villum Kann Rasmusssen Fund (VKR) and The Danish Natural Science Research Council (FNU).

Appendix A. Supplementary material

Tables S1 and S2 of the Supplementary material tabulate the electronic and zero-point vibrational energies of the discussed structures. The moments of inertia and vibrational frequencies are summarized in the Tables S3–S6. Supplementary data associated with this article can be found, in the online version, at doi:10.1016/j.cplett.2010.03.031.

References

[1] H. Roper, Starch-Starke 54 (2002) 89.
[2] J. Hill, E. Nelson, D. Tilman, S. Polasky, D. Tiffany, Proc. Natl. Acad. Sci. USA 103 (2006) 11206.
[3] P.J. Crutzen, A.R. Mosier, K.A. Smith, W. Winiwarter, Atmos. Chem. Phys. 8 (2008) 389.
[4] European Biodiesel Board <www.ebb-eu.org>.
[5] K. Bendtz, EU-25 Oilseeds and producs: Biofuels situation in the European Union 2005, GAIN report, USDA and Foreign Agricultural Service, Washington, DC, 2005.
[6] Worldwatch Institute, Biofuel for Transport, Earthscan, London, 2007.
[7] T.J. Wallington, E.W. Kaiser, J.T. Farrell, Chem. Soc. Rev. 35 (2006) 335.
[8] J.P. Szybist, J. Song, M. Alam, A.L. Boehman, Fuel Process. Technol. 88 (2007) 679.
[9] J.R. Pedersen, A. Ingemarsson, J.O. Olsson, Chemosphere 38 (1999) 2467.
[10] M.Z. Jacobson, Environ. Sci. Technol. 41 (2007) 4150.
[11] E.S.C. Kwok, R. Atkinson, Atmos. Environ. 29 (1995) 1685.
[12] O.J. Nielsen, T.J. Wallington, J. Platz, Reaction of OH with oxygenated compounds, in: Proceeding from the EUROTRAC-2 Symposium, 2002.
[13] V.F. Andersen, E.J.K. Nilsson, S. Jørgensen, O.J. Nielsen, M.S. Johnson, Chem. Phys. Lett. 472 (2009) 23.
[14] A. El Boudali, S. Le Calve, G. Le Bras, J. Mellouki, J. Phys. Chem. 100 (1996) 12364.
[15] D.F. Smith, C.D. Mciver, T.E. Kleindienst, Int. J. Chem. Kinet. 27 (1995) 453.
[16] T.J. Wallington, P. Dagaut, R.H. Liu, M. Kurylo, Int. J. Chem. Kinet. 20 (1998) 177.
[17] I.M. Campbell, P.E. Parkinson, Chem. Phys. Lett. 5 (1978) 385.
[18] L. Yang, J.Y. Liu, Z.S. Li, J. Phys. Chem. A 112 (2008) 6364.
[19] M.J. Frisch et al., Gaussian 03, Revision C.02, Gaussian Inc., Wallingford, CT, 2004.
[20] C.T. Lee, W.T. Yang, R.G. Parr, Phys. Rev. B 37 (1988) 785.
[21] A.D. Becke, J. Chem. Phys. 98 (1993) 1372.
[22] W.J. Hehre, R. Ditchfield, J.A. Pople, J. Chem. Phys. 56 (1972) 2257.
[23] M.J. Frisch, J.A. Pople, J.S. Binkley, J. Chem. Phys. 80 (1984) 3265.
[24] T.H. Dunning, J. Chem. Phys. 90 (1989) 1007.
[25] J.L. Durant, Chem. Phys. Lett. 256 (1996) 595.
[26] C. Gonzalez, H.B. Schlegel, J. Chem. Phys. 90 (1989) 2154.
[27] C. Gonzalez, H.B. Schlegel, J. Phys. Chem. 94 (1990) 5523.
[28] W.J. Hehre, L. Radom, R.R. Schleyer, J.A. Pople, Ab-initio Molecular Orbital Theory, Wiley, New York, 1986.
[29] J.A. Pople, M. Head-Gordon, K. Raghavachari, J. Chem. Phys. 87 (1987) 5968.
[30] J.R. Alvarez-Idaboy, I. Diaz-Acosta, A. Vivier-Bunge, J. Comp. Chem. 19 (1998) 811.
[31] L.A. Curtiss, K. Raghavachari, P.C. Redfern, V. Rassolov, J.A. Pople, J. Chem. Phys. 109 (1998) 7764.
[32] J.A. Montgomery Jr., M.J. Frisch, J.W. Ochterski, G.A. Petersson, J. Chem. Phys. 110 (1999) 2822.
[33] J.A. Montgomery Jr., M.J. Frisch, J.W. Ochterski, G.A. Petersson, J. Chem. Phys. 112 (2000) 6532.
[34] D.A. McQuarrie, Statistical Mechanics, Harper Collins Publisher, New York, 1976.
[35] M.W. Chase Jr., C.A. Davies, J.R. Downey Jr., D.J. Frurip, R.A. McDonald, A.N. Syverud, JANAF Thermochemical Table, thrid edn., vol. 14, National Bureau of Standards, Washington, DC, 1985.
[36] E. Wigner, Z. Phys. Chem.-Abteilung B-Chem. Der Elementarprozesse Aufbau Der Materie 19 (1932) 203.
[37] W.F. Lei, R.Y. Zhang, W.S. McGivern, A. Derecskei-Kovacs, S.W. North, Chem. Phys. Lett. 326 (2000) 109.